Green Chemistry

PAPER

View Article Online
View Journal | View Issue

Cite this: *Green Chem.*, 2025, **27**, 2065

Promoting H_2O_2 direct synthesis through Fe incorporation into AuPd catalysts†

Rong-Jian Li,‡[a] Richard J. Lewis, *‡[a] Ángeles López-Martín,[a] David J. Morgan, [a,b] Thomas E. Davies,[a] David Kordus,[c] A. Iulian Dugulan,[d] Beatriz Roldan Cuenya [c] and Graham J. Hutchings *[a]

Received 10th January 2025,
Accepted 16th January 2025

DOI: 10.1039/d5gc00134j

rsc.li/greenchem

In recent years growing interest has been placed on the role of dopant concentrations of tertiary precious and base metals in modifying the performance of supported AuPd nanoalloys towards the direct synthesis of H_2O_2. Within this contribution, we expand on these earlier studies, with a focus on Fe-containing systems. Through rational catalyst design, an optimal 0.5%Au–0.5%Pd–0.02%Fe/TiO_2 formulation has been developed, which not only outperforms the parent bimetallic analogue but also offers increased reactivity compared to alternative trimetallic formulations previously reported, including those which incorporate Pt. Such observations may be surprising given the propensity for Fe to decompose H_2O_2 *via* Fenton pathways. However, detailed analysis by CO-DRFITS and XPS reveals that the enhanced activity can be attributed to the electronic modification of Pd and the formation of domains of mixed Pd^{2+}/Pd^0 oxidation state, upon Fe introduction. Notably, the resulting improvement in catalytic performance which results from dopant Fe incorporation, is seen to result from an increase in H_2 utilisation, rather than improved catalytic selectivity towards H_2O_2.

Green Foundation

(1) To date, despite the improved catalytic performance that results from their application, the investigation of tertiary metal modifiers into AuPd nanoalloys in H_2O_2 direct synthesis, has largely been restricted to precious metals, such as Pt.
(2) This work demonstrates that through the incorporation of Fe considerable improvements in reactivity, may be achieved, with the optimised AuPdFe catalyst outperforming both the parent AuPd material and Pt-based analogues.
(3) Further catalyst design is required to ensure that the increased reactivity of the catalyst does not result from compromises in selectivity towards H_2O_2.

Introduction

The direct synthesis of H_2O_2 from the elements represents an attractive alternative to the current industrial route to producing this powerful, environmentally friendly oxidant, the Anthraquinone Oxidation (AO) Process, theoretically offering total atomic efficiency and allowing for localised production. In particular, the direct route may find the greatest application for transformations which rely on the continual *in situ* supply of low levels of the oxidant,[1–3] and where the presence of the proprietary stabilisers present in commercial, preformed H_2O_2 would preclude application.[4]

In recent years a growing number of catalyst formulations have been reported that offer near-total selectivity towards H_2O_2,[5–9] overcoming one of the major hurdles that have prevented industrial adoption of the direct route; the undesirable degradation of H_2O_2 to H_2O *via* decomposition and hydrogenation pathways. However, for the direct approach to be competitive with the AO Process, H_2O_2 concentrations of approximately 5 vol% must be obtained to minimise the energy requirements associated with product separation and concentration prior to shipping. To date, such concentrations have only been achieved through the use of H_2/O_2 gas mixtures within the explosive regime, which is clearly not practical at scale.

[a]*Max Planck-Cardiff Centre on the Fundamentals of Heterogeneous Catalysis FUNCAT, Cardiff Catalysis Institute, School of Chemistry, Cardiff University, Translational Research Hub, Maindy Road, Cardiff, CF24 4HQ, UK. E-mail: LewisR27@Cardiff.ac.uk, Hutch@Cardiff.ac.uk*
[b]*HarwellXPS, Research Complex at Harwell (RCaH), Didcot, OX11 OFA, UK*
[c]*Department of Interface Science, Fritz Haber Institute of the Max Planck Society, 14195 Berlin, Germany*
[d]*Laboratory of Fundamentals Aspects of Materials and Energy, Department of Radiation Science & Technology, Delft University of Technology, Mekelweg 15, 2628 CD Delft, The Netherlands*

†Electronic supplementary information (ESI) available. See DOI: https://doi.org/10.1039/d5gc00134j

‡These authors contributed equally to this work.

To address performance limitations the introduction of a growing number of secondary metal promoters into supported Pd-catalysts has been studied,[6,10–12] with AuPd-based systems perhaps attracting the greatest attention,[13–15] with the synergistic enhancements that result from the formation of AuPd alloys considerable and often attributed to a combination of electronic and isolation effects, with the disruption of contiguous Pd domains, widely considered to be key in preventing the cleavage of the O–O bond (in $*O_2$, $*H_2O_2$, or *OOH) and the resultant formation of H_2O.

By comparison, the use of trimetallic formulations for the direct synthesis of H_2O_2 has received far less attention, although there are growing reports of the enhanced performance which can be achieved through the introduction of low quantities of dopant promoters, particularly into AuPd nanoalloys. Building on early work which focussed on AuPdPt systems,[16,17] attention has recently shifted towards the use of more abundant transition metals as promoters for AuPd species, which have identified the promotive role of Cu, Zn and Ni dopants in the direct synthesis reaction, with optimised formulations offering improved reactivity compared to AuPdPt analogues.[18,19] Based on these earlier we now turn our attention to the role of Fe as a promoter for AuPd catalysts.

Experimental

Catalyst preparation

A series of bi- and tri-metallic 1%AuPd–*X*%Fe/TiO_2 (X = 0.01–1.0) catalysts have been prepared by a wet co-impregnation procedure, based on a methodology previously reported in the literature.[16] The procedure to produce the 0.5%Au–0.5%Pd–1%Fe/TiO_2 catalyst (2 g) is outlined below, in all cases the Au : Pd ratio is 1 : 1 (wt/wt), with a similar methodology to that outlined below utilised for all catalysts investigated.

Aqueous solutions of $HAuCl_4{\cdot}3H_2O$ (0.806 mL, [Au] = 12.4 mg mL^{-1}, Strem Chemicals), $PdCl_2$ (1.713 mL, [Pd] = 5.8 mg mL^{-1}, Sigma Aldrich) and $FeCl_3$ (0.0599 g, Sigma Aldrich) were mixed in a 50 mL round bottom flask and heated to 65 °C with stirring (1000 rpm) in a thermostatically controlled oil bath, with total volume fixed to 16 mL using H_2O (HPLC grade, Fischer Scientific). Upon reaching 65 °C, TiO_2 (1.96 g, P25, Degussa) was added over the course of 10 minutes with constant stirring. The resulting slurry was stirred at 65 °C for a further 15 min, following this the temperature was raised to 85 °C for 16 h to allow for complete evaporation of water. The resulting solid was ground prior to heat treatment in a reductive atmosphere (5%H_2/Ar, 400 °C, 4 h, 10 °C min^{-1}).

Catalyst testing

Note 1: reaction conditions used within this study operate under the flammability limits of gaseous mixtures of H_2 and O_2.

Note 2: the conditions used within this work for H_2O_2 synthesis and degradation have previously been investigated, with the presence of CO_2 as a diluent for reactant gases and a methanol co-solvent identified as key to maintaining high catalytic efficacy towards H_2O_2 production.[20] In particular the CO_2 gaseous diluent, has been found to act as an *in situ* promoter of H_2O_2 stability through dissolution in the reaction medium and the formation of carbonic acid. We have previously reported that the use of the CO_2 diluent has a comparable promotive effect to that observed when acidifying the reaction solution to a pH of 4 using HNO_3.[21]

Regarding the choice of the solvent alcohol-based solvents have been widely studied for the direct synthesis of H_2O_2, in part this choice is due to the improved solubility of gaseous reagents, compared to that in water, and assist in preventing mass transfer limitations. However, more recently, Flaherty and co-workers have demonstrated the direct involvement of the solvent within the direct synthesis mechanism, which resembles the two-electron oxygen reduction reaction (ORR), where H_2O_2 is formed by kinetically relevant proton (from solvent molecules)—electron (provided by heterolytic hydrogen oxidation, $H_2 \leftrightarrow 2H^+ + 2e^-$) transfer to surface-bound hydroperoxy intermediates. The reader is directed to the seminal work by Flaherty and co-workers for an in-depth discussion of the H_2O_2 direct synthesis mechanism.[22]

Direct synthesis of H_2O_2

Hydrogen peroxide synthesis was evaluated using a Parr Instruments stainless steel autoclave with a nominal volume of 100 mL, equipped with a PTFE liner so that the total volume is reduced to 66 mL, and a maximum working pressure of 2000 psi. To test each catalyst for H_2O_2 synthesis, the autoclave liner was charged with catalyst (0.01 g) and solvent (methanol (5.6 g, HPLC grade, Fischer Scientific) and H_2O (2.9 g, HPLC grade, Fischer Scientific)). The charged autoclave was then purged three times with 5%H_2/CO_2 (100 psi) before filling with 5%H_2/CO_2 to a pressure of 420 psi, followed by the addition of 25%O_2/CO_2 (160 psi), with the pressure of 5%H_2/CO_2 and 25%O_2/CO_2 given as gauge pressures. The reactor was not continually fed with reactant gases. The reaction was conducted at a temperature of 2 °C for 0.5 h with stirring (1200 rpm). The above reaction parameters are based on optimum conditions we have previously reported for the synthesis of H_2O_2. H_2O_2 productivity was determined by titrating aliquots of the final solution after reaction with acidified $Ce(SO_4)_2$ (0.0085 M) in the presence of ferroin indicator. Catalyst productivities are reported as $mol_{H_2O_2}$ kg_{cat}^{-1} h^{-1}. To collect a series of data points, as in the case of Fig. 3, it should be noted that individual experiments were carried out and the reactant mixture was not sampled on-line.

The catalytic conversion of H_2 and selectivity towards H_2O_2 were determined using a Varian 3800 GC fitted with TCD and equipped with a Porapak Q column.

H_2 conversion (eqn (1)) and H_2O_2 selectivity (eqn (2)) are defined as follows:

$$H_2\ \text{conversion}\ (\%) = \frac{\text{mmol}_{H_2(t(0))} - \text{mmol}_{H_2(t(1))}}{\text{mmol}_{H_2(t(0))}} \times 100 \quad (1)$$

$$H_2O_2\ \text{selectivity}\ (\%) = \frac{H_2O_2\ \text{detected (mmol)}}{H_2\ \text{consumed (mmol)}} \times 100 \quad (2)$$

The total autoclave capacity was determined *via* water displacement to allow for accurate calculation of H_2 conversion and H_2O_2 selectivity. When equipped with the PTFE liner the total volume of an unfilled autoclave was determined to be 93 mL, which includes all available gaseous space within the autoclave.

Gas replacement experiments for the direct synthesis of H_2O_2

An identical procedure to that outlined above for the direct synthesis reaction was followed for a reaction time of 0.5 h. After this, stirring was stopped and the reactant gas mixture was vented prior to replacement with the standard pressures of 5%H_2/CO_2 (420 psi) and 25%O_2/CO_2 (160 psi). The reaction mixture was then stirred (1200 rpm) for a further 0.5 h. To collect a series of data points, as in the case of Fig. 7, it should be noted that individual experiments were carried out and the reactant mixture was not sampled on-line.

Degradation of H_2O_2

Catalytic activity towards H_2O_2 degradation was determined in a similar manner to the direct H_2O_2 synthesis activity of a catalyst. The autoclave liner was charged with solvent (methanol (5.6 g, HPLC grade, Fischer Scientific) and H_2O (2.21 g, HPLC grade, Fischer Scientific)) and H_2O_2 (50 wt% 0.69 g, Sigma Aldrich), with the solvent composition equivalent to 4 wt% H_2O_2. From the solution, two 0.05 g aliquots were removed and titrated with acidified $Ce(SO_4)_2$ solution using ferroin as an indicator to determine an accurate concentration of H_2O_2 at the start of the reaction. Subsequently the catalyst (0.01 g) was added to the reaction media and the autoclave was purged with 5%H_2/CO_2 (100 psi) prior to being pressurised with 5% H_2/CO_2 (420 psi). The reaction medium was cooled to a temperature of 2 °C, prior to stirring (1200 rpm) for 0.5 h. After the reaction was complete the catalyst was removed from the reaction mixture and two 0.05 g aliquots were titrated against the acidified $Ce(SO_4)_2$ solution using ferroin as an indicator. The degradation activity is reported as $mol_{H_2O_2}\ kg_{cat}^{-1}\ h^{-1}$.

Catalyst reusability in the direct synthesis and degradation of H_2O_2

In order to determine catalyst reusability, a similar procedure to that outlined above for the direct synthesis of H_2O_2 was followed utilising 0.05 g of catalyst. Following the initial test, the catalyst was recovered by filtration, washed with DI water, and dried (30 °C, 16 h, under vacuum); from the recovered catalyst sample 0.01 g was used to conduct a standard H_2O_2 synthesis or degradation test, as outlined above.

Note 3: in all cases the reactor temperature was controlled using a HAAKE K50 bath/circulator using an appropriate coolant.

In all cases reactions were run multiple times, a minimum of three, over multiple batches of catalyst, a minimum of two, with the data being presented as an average of these experiments. The catalytic activity toward the direct synthesis and subsequent degradation of H_2O_2 was found to be consistent to within ±2% on the basis of multiple reactions.

Characterisation

X-ray photoelectron spectroscopy (XPS) measurements were performed on a Kratos Axis Ultra-DLD photoelectron spectrometer utilising monochromatic Al K_α X-ray source operating at 144 W (12 mA × 12 kV). Samples were pressed onto silicone free double sizded Scotch tape, and analysed using the hybrid spectroscopy mode, giving an analysis area of *ca.* 700 × 300 microns. High resolution and survey spectra were acquired at pass energies of 40 eV (step size 0.1 eV) and 160 eV (step size 1 eV) respectively. Charge compensation was performed using low energy electrons and the resulted spectrum calibrated to the lowest C(1s) peak from the fitted carbon core-level spectra, taken to be 284.8 eV. The suitability of the C(1s) referencing was confirmed by a secondary reference point, taken to be the Ti($2p_{3/2}$) peak with a binding energy of 458.7 eV, characteristic of that for virgin TiO_2. All data was processed using CasaXPS v2.3.24 using a Shirley background and modified Wagner factors as supplied by the instrument manufacturer. Peak fits were performed using a combination of Voigt-type functions (LA line shape in CasaXPS) andmodels derived from bulk reference samples where appropriate.

The bulk structure of the catalysts was determined by powder X-ray diffraction using a (θ–θ) PANalytical X'pert Pro powder diffractometer using a Cu K_α radiation source, operating at 40 keV and 40 mA. Standard analysis was carried out using a 40 min run with a back filled sample, between 2θ values of 20–80°. Phase identification was carried out using the International Centre for Diffraction Data (ICDD).

Note 4: X-ray diffractograms of the as-prepared catalysts are reported in Fig. S1,† with no reflections associated with active metals, indicative of the relatively low total loading of the immobilised metals.

Transmission electron microscopy (TEM) was performed on a JEOL JEM-2100 operating at 200 kV. Samples were prepared by dispersion in ethanol by sonication and deposited on 300 mesh copper grids coated with holey carbon film. To allow for the determination of mean particle size, a minimum of 300 particles were measured. Aberration-corrected scanning transmission electron microscopy (AC-STEM) was performed using a probe-corrected Hitachi HF5000 S/TEM, operating at 200 kV. The instrument was equipped with bright field (BF), high angle annular dark field (HAADF) and secondary electron (SE) detectors for high spatial resolution STEM imaging experiments. This microscope was also equipped with a secondary electron detector and dual Oxford Instruments XEDS detectors (2 × 100 mm^2) having a total collection angle of 2.02 sr. Energy dispersive X-ray spectroscopy (XEDS) was performed using an Oxford Instruments X-Max^N 80 detector and the data analysed using Aztec software.

Transmission ^{57}Fe Mössbauer spectra were collected at 50 and 4.2 K with a conventional constant-acceleration spectrometer using a ^{57}Co(Rh) source. Velocity calibration was carried

out using an α-Fe foil at room temperature. The Mössbauer spectra were fitted using the Mosswinn 4.0 program.[23]

CO-DRIFTS measurements were taken on a Bruker Tensor 27 spectrometer fitted with a mercury cadmium telluride (MCT) detector. The sample was loaded into the Praying Mantis high temperature (HVC-DRP-4) *in situ* cell before exposure to N_2 and then 1% CO/N_2 at a flow rate of 50 cm^3 min^{-1}. A background spectrum was obtained using KBr, and measurements were recorded every 1 min at room temperature. Once the CO adsorption bands in the DRIFT spectra ceased to increase in intensity, the gas feed was changed back to N_2, in order to evacuate gaseous CO. Measurements were repeated until no change in subsequent spectra was observed.

Total metal leaching from the supported catalyst was quantified *via* inductively coupled plasma mass spectrometry (ICP-MS). Post-reaction solutions were analysed using an Agilent 7900 ICP-MS equipped with I-AS auto-sampler. All samples were diluted by a factor of 10 using HPLC grade H_2O (1%HNO_3 and 0.5% HCl matrix). All calibrants were matrix-matched and measured against a five-point calibration using certified reference materials purchased from PerkinElmer and certified internal standards acquired from Agilent.

To allow for quantification of total metal loading catalytic samples were digested *via* an aqua-regia-assisted microwave digestion method using a Milestone Connect Ethos UP microwave with an SK15 sample rotor. Digested samples were analysed by inductively coupled plasma–optical emission spectroscopy (ICP-MS). All calibrants were matrix-matched and measured against a five-point calibration using certified reference materials purchased from PerkinElmer and certified internal standards acquired from Agilent. Actual metal loadings of key catalytic samples are provided in Table S1.†

Results and discussion

Under conditions that have previously been optimised to ensure H_2O_2 stability,[20] our initial investigations established the ability of dopant concentrations of Fe to promote the performance of AuPd-based catalysts towards H_2O_2 production (Fig. 1A), with the optimal 0.5%Au–0.5%Pd–0.02%Fe/TiO_2 formulation achieving rates of H_2O_2 synthesis (122 $mol_{H_2O_2}$ kg^{-1} cat^{-1}), far greater than that offered by the parent 0.5%Au–0.5% Pd/TiO_2 catalyst (70 $mol_{H_2O_2}$ kg^{-1} cat^{-1}). Interestingly, catalytic activity towards H_2O_2 degradation was found to follow a similar trend to that observed for H_2O_2 synthesis, with both metrics reaching a maximum at a Fe loading of 0.02 wt%, before decreasing considerably with further Fe incorporation. Notably, the high Fe-loaded 0.5%Au–0.5%Pd–1%Fe/TiO_2 catalyst was found to offer H_2O_2 synthesis rates (65 $mol_{H_2O_2}$ kg^{-1} cat^{-1}), somewhat lower than that observed over the bimetallic parent catalyst. Determination of catalytic selectivity towards H_2O_2 and H_2 conversion during H_2O_2 synthesis is presented in Fig. 1B, with these measurements, alongside our evaluation of H_2O_2 synthesis and degradation activity (Fig. 1A), revealing that the improved performance that results from the introduction of dopant quantities of Fe can be primarily associated with increased rates of H_2 utilisation (an indicator of catalytic activity), rather than through an enhancement in H_2O_2 selectivity. The improved performance of the 0.5%Au–0.5%Pd–0.02% Fe/TiO_2 catalyst is further highlighted through a comparison of calculated reaction rates (Table S2†), at a reaction time (5 minutes), where it may be assumed (1) that there is no contribution from subsequent H_2O_2 degradation reactions and (2) that the reaction is not limited by gaseous reagent availability.

Evaluation of the as-prepared AuPdFe/TiO_2 catalysts by X-ray photoelectron spectroscopy (XPS) is shown in Fig. 2 and reveals the presence of a significant proportion of Pd^{2+} for all formulations, despite the exposure of the catalysts to a rela-

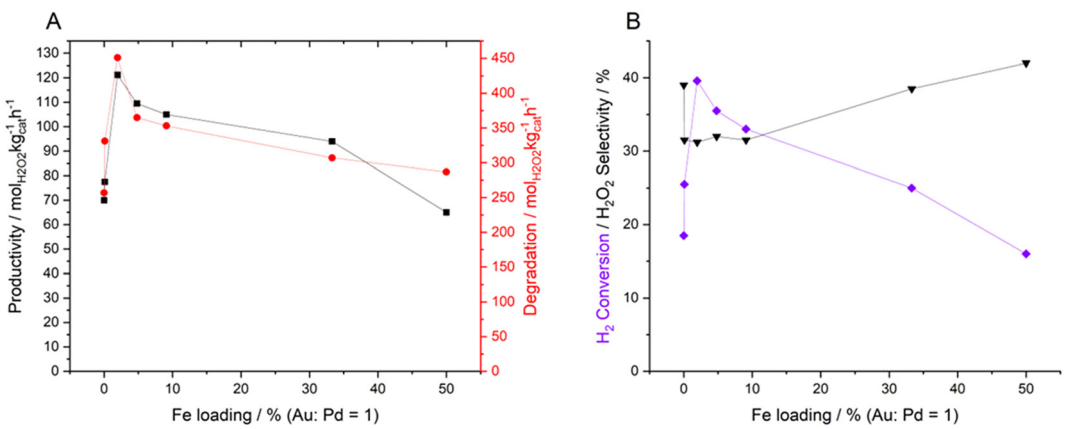

Fig. 1 The effect of Fe loading on the performance of 1%AuPd/TiO_2 catalysts towards (A) the direct synthesis and subsequent degradation of H_2O_2, with a determination of H_2 and H_2O_2 selectivity during H_2O_2 synthesis shown in (B). *Key*: H_2O_2 synthesis (black squares), H_2O_2 degradation (red circles), H_2 conversion (black inverted triangles), H_2O_2 selectivity (purple diamonds) H_2O_2 direct synthesis reaction conditions: catalyst (0.01 g), H_2O (2.9 g), MeOH (5.6 g), 5% H_2/CO_2 (420 psi), 25% O_2/CO_2 (160 psi), 0.5 h, 2 °C 1200 rpm. H_2O_2 degradation reaction conditions: catalyst (0.01 g), H_2O_2 (50 wt% 0.69 g) H_2O (2.21 g), MeOH (5.6 g), 5% H_2/CO_2 (420 psi), 0.5 h, 2 °C 1200 rpm. *Note*: additional data is reported in Table S2.†

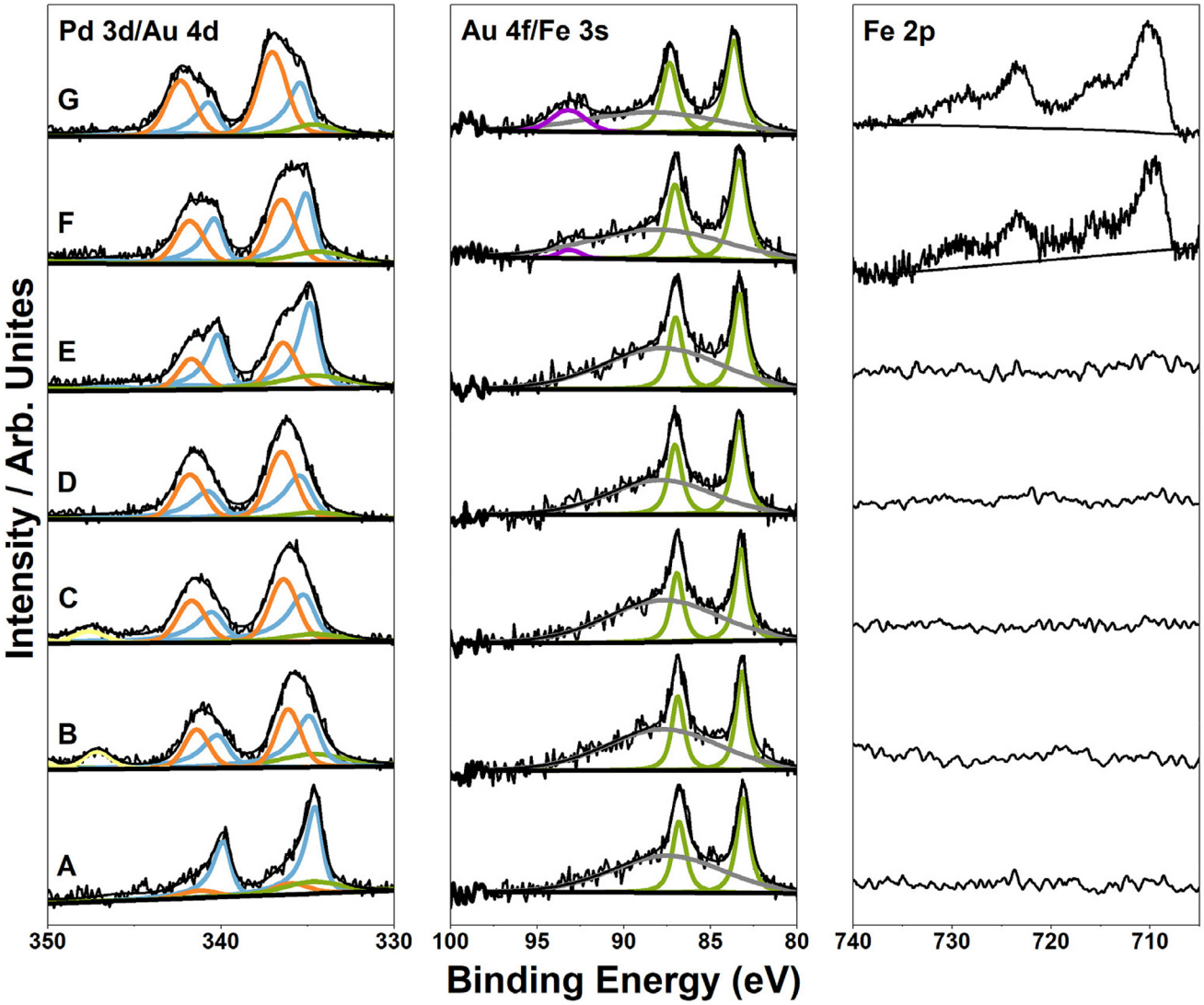

Fig. 2 XPS analysis of the as-prepared AuPdFe/TiO_2 catalysts. (A) 0.5%Au–0.5%Pd/TiO_2, (B) 0.5%Au–0.5%Pd–0.01%Fe/TiO_2, (C) 0.5%Au–0.5%Pd–0.02%Fe/TiO_2, (D) 0.5%Au–0.5%Pd–0.05%Fe/TiO_2, (E) 0.5%Au–0.5%Pd0.1%Fe/TiO_2, (F) 0.5%Au–0.5%Pd–0.5%Fe/TiO_2 and (G) 0.5%Au–0.5%Pd–1.0%Fe/TiO_2. *Key*: Au(4d) & Au(4f) (green); Fe(3s) (purple); Pd^0 (blue); Pd^{2+} (orange); loss of structure (grey); Ca^{2+} (yellow). *Note 1*: catalysts exposed to a reductive heat treatment prior to use (5%H_2/Ar, 400 °C, 4 h, 10 °C min^{-1}). *Note 2*: Ca^{2+} signal results from the use of distilled water during catalyst preparation.

tively high-temperature reductive heat treatment (5%H_2/Ar, 400 °C, 4 h, 10 °C min^{-1}), likely in part due to preparation for analysis under standard laboratory conditions. However, it is evident the incorporation of Fe results in a clear shift in Pd speciation, towards Pd^{2+}, with such observations aligning well with our earlier studies investigating the role of alternative transition metals as promoters for AuPd nanoalloys.[18,19] Notably, the performance of Pd-based catalysts towards H_2O_2 synthesis is well known to be highly dependent on Pd oxidation state, with domains of mixed Pd^{2+}–Pd^0 species typically offering improved performance compared to those with a predominance of Pd in either oxidation state.[24] As such, it is possible, at least in part, to attribute the improved activity, which results from the incorporation of dopant levels of Fe into AuPd alloys to the control of Pd speciation. In the case of the Fe speciation, we observe a distinct signal at a binding energy of 710.8 eV and satellite structure at *ca.* 719 eV, characteristic of Fe^{3+}. However, here we wish to highlight the propensity of Fe to readily oxidise under ambient conditions and the surface sensitivity of XPS. The broadness of the Fe 2p core-level spectra suggests a lower oxidation state could be present, as such, we cannot rule out the presence of lower Fe oxidation states based on XPS analysis alone. Additionally, it should also be noted that active metal speciation of the as-prepared materials is likely not fully representative of those under reaction conditions.

With our evaluation by XPS unable to provide sufficient information about the nature of the Fe in the AuPdFe formulations, we subsequently employed ^{57}Fe Mössbauer spectroscopic analysis to gain further insight. Notably, these samples

contain identical Fe loadings as analogues investigated for H_2O_2 synthesis but were prepared with $^{57}FeCl_3$ as the metal precursor, with comparisons made to a monometallic 0.02%$^{57}Fe/TiO_2$ formulation (Table 1 and Fig. 3).

Interestingly, the spectra of the monometallic Fe sample (0.02%Fe/TiO_2) were fitted with contributions of Fe^{2+} only, aligning with earlier works by Vanleerberghe *et al.*,[25] and indicative of the strong interaction between the immobilised Fe and TiO_2 support, possibly through the formation of iron titanates. By comparison, the spectra of the trimetallic 0.5% Au–0.5%Pd–0.02%Fe/TiO_2 formulation is far more complex. In addition to the Fe^{2+} (iron titanate) species observed in the monometallic Fe sample, contributions indicative of a Fe–Pd (Au) phase (magnetic (sextuplet) contribution of 31.4 T), isolated Fe^{3+} species (paramagnetic doublet at 4.2 K) and Fe^{3+} oligomers (broad sextuplet) are also visible. Notably, these Fe^{3+} species were not present in the 0.02%Fe/TiO_2 sample, further indicating the electronic interaction between Fe and the precious metals. Additionally, Au/Pd–Fe dimers (paramagnetic doublet) and Au–Pd–Fe oligomers (broad sextuplet) were also found to be present, aligning well with earlier investigations into AuFe structures.[26] Contrastingly, the spectra of the 0.5% Au–0.5%Pd–1.0%Fe/TiO_2 sample was dominated by isolated and oligomeric Fe^{3+} species, in addition to contributions from the iron (Fe^{2+}) titanate species observed in alternative formulations, with minor contributions from Fe^0. Notably, we were unable to observe the Fe–Pd(Au) phase present in the optimal 0.5%Au–0.5%Pd–0.02%Fe/TiO_2 formulation.

Returning to our non-isotopically labelled samples CO-DRFITS was subsequently employed to further probe the electronic interaction that results from the incorporation of Fe into AuPd nanoalloys (Fig. S2,† which includes CO-DRIFTS analysis of a 1%Fe/TiO_2 catalyst for comparative purposes). Perhaps unsurprisingly, given the low loading of Fe in the 0.5%Au–0.5%Pd–0.02%Fe/TiO_2 catalyst, no clear variation in the DRIFTS spectra was observed between the optimal trimetallic catalyst and bimetallic AuPd analogue, with both spectra dominated by Pd-CO bands. The bands observed at approximately 2060 cm^{-1} represent CO bonded linearly to low co-ordination Pd sites (*i.e.* edge or corner sites, denoted Pd-CO), while the broad feature, which is centred around 1925 cm^{-1} represents the 2- and 3-fold adsorption of CO on Pd.[27,28] Notably, no bands associated with the adsorption of CO onto the TiO_2 support (>2200 cm^{-1} and previously reported by Cerrato *et al.*[29] and Green *et al.*[30]) or gaseous CO_2 (2350 cm^{-1})[31] were observed, likewise we do not observe bands which may be associated with the redox process of FeOx, (typically at 3700 cm^{-1}).[32] Interestingly upon the introduction of large quantities of Fe, a clear red-shift in the bands related to the linearly bonded CO on Pd and the bridging CO species can be observed, which may be attributed to charge-transfer to Pd d-orbitals, resulting in an enhanced back donation to 2π CO molecular orbitals, such observations align well with our earlier analysis by XPS which indicated the electronic modification of Pd species as a result of Fe incorporation.

Further analysis of the as-prepared catalytic series by transition electron microscopy (TEM), prior to use in the H_2O_2 direct synthesis reaction, is reported in Table 2 (representative micrographs are reported in Fig. S3†). A minimal variation in this metric was observed across the catalytic series, with a mean particle size between 2 and 5 nm observed for the parent AuPd, and Fe-containing trimetallic formulations. While such measurements were conducted on fresh materials (*i.e.* prior to use in the direct synthesis reaction), it is considered that they reveal no direct correlation between catalytic performance and particle size or nanoparticle dispersion. As such it may be reasonable to conclude that the improved reactivity that results from the incorporation of dopant concentrations of Fe may be attributed to the electronic modification of Pd species, as indicated by our XPS and CO-DRIFTS analysis.

The observation of a strong dependency between Fe content and catalytic performance in the H_2O_2 synthesis reaction, and the enhanced catalytic activity of key formulations compared to those previously reported in the literature (Table S3†),

Table 1 The Mössbauer fitted parameters of the AuPd$^{57}Fe/TiO_2$ samples, obtained at different temperatures

Sample	*T* (K)	IS (mm s^{-1})	QS (mm s^{-1})	Hyperfine field (T)	*Γ* (mm s^{-1})	Phase	Spectral contribution (%)
0.02%$^{57}Fe/TiO_2$	4.2	1.09	2.08	—	0.67	Fe^{2+} (red)	37
		1.29	2.49	—	0.71	Fe^{2+} (blue)	63
Au–Pd–0.02%$^{57}Fe/TiO_2$	4.2	0.37	0.02	31.4	0.64	Fe–Pd(Au) (red)	18
		1.32	2.62	—	1.20	Fe^{2+} (magenta)	19
		0.59	−0.14	40.9	1.21	Fe^{3+} (oligomers) (blue)	41
		0.49	0.93	—	0.97	Fe^{3+} (isolated) (green)	22
Au–Pd–1%$^{57}Fe/TiO_2$	4.2	0.13	0.00	34.0	0.36	Fe^0 (red)	6
		1.12	2.63	—	1.20	Fe^{2+} (magenta)	14
		0.58	−0.15	37.7	1.27	Fe^{3+} (oligomers) (blue)	35
		0.51	0.79	—	0.70	Fe^{3+} (isolated) (green)	45
Au–Pd–1%$^{57}Fe/TiO_2$	50	0.11	0.00	33.9	0.36	Fe^0 (red)	10
		1.10	2.51	—	0.71	Fe^{2+} (magenta)	19
		0.50	0.78	—	0.60	Fe^{3+} (oligomers) + Fe^{3+} (isolated) (green)	71

Experimental uncertainties: isomer shift: I.S. ± 0.1 mm s^{-1}; quadrupole splitting: Q.S. ± 0.2 mm s^{-1}; line width: *Γ* ± 0.2 mm s^{-1}; hyperfine field: ± 0.2 T; spectral contribution: ± 5%.

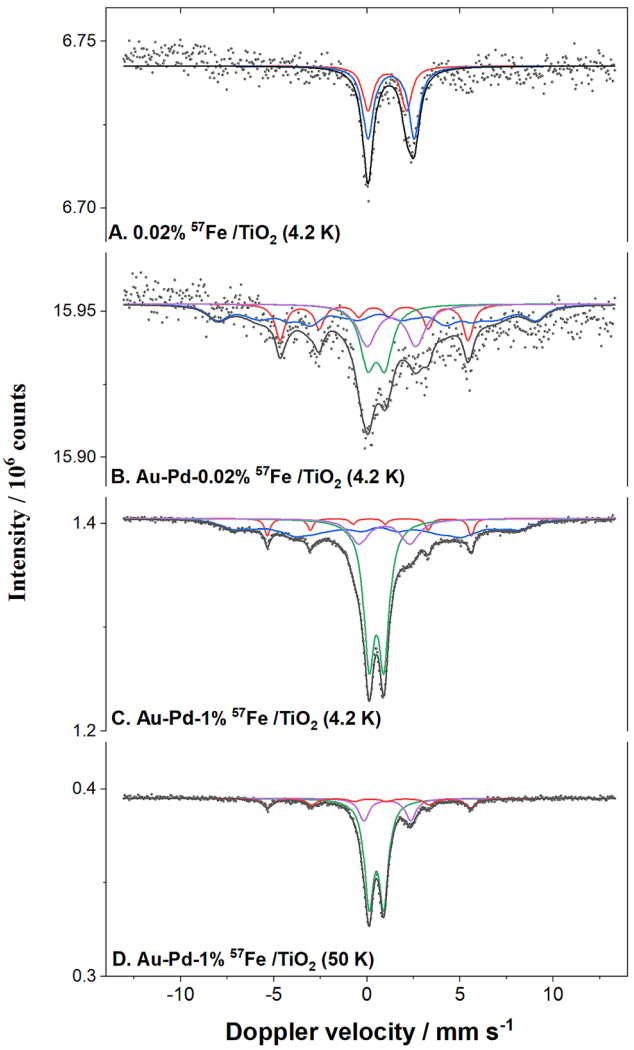

Fig. 3 Mössbauer analysis of the AuPd^{57}Fe/TiO$_2$ samples at different temperatures; (A) 0.02%^{57}Fe/TiO$_2$ (B) 0.5%Au–0.5%Pd–0.02%^{57}Fe/TiO$_2$ and (C-D) 0.5%Au–0.5%Pd–1%Fe/TiO$_2$. *Note*: analysis temperatures reported in parentheses, phase identification is reported in Table 1.

motivated us to further investigate the structure–activity relationships existing over the 0.5%Au–0.5%Pd/TiO$_2$, 0.5%Au–0.5%Pd–0.02%Fe/TiO$_2$ and 0.5%Au–0.5%Pd–1%Fe/TiO$_2$ catalysts. While our initial studies (Fig. 1) indicated that the incorporation of Fe resulted in a loss of selectivity towards H_2O_2, it is important to highlight that the catalytic series was not compared at near-equivalent rates of H_2 conversion. Subsequent evaluation of H_2O_2 selectivity of key catalyst formulations at near iso-conversion is reported in Table S4,† from which it is clear that the incorporation of dopant concentrations of Fe (0.02 wt%) does indeed reduce catalytic selectivity (41% selectivity at 9% H_2 conversion), compared to that offered by the parent bimetallic analogue (50% selectivity at 8% H_2 conversion). However, the extent of this reduction is not as substantial as that which may be inferred from the data reported in Fig. 1. Regardless, from such comparisons and previous observations, it is possible to conclude that the enhanced performance of the 0.5%Au–0.5%Pd–0.02%Fe/TiO$_2$ catalyst is indeed associated with increased activity, rather than a promotion of catalytic selectivity towards H_2O_2.

Analysis of key catalyst formulations *via* STEM-HAADF imaging (Fig. 4, with additional data reported in Fig. S.4†) corroborated our earlier investigation by TEM (Table 2 and Fig. S3†) which indicated the minimal variation in particle size across the wider catalyst series. Corresponding EDX mapping further revealed the intimate alloying of active metals (Fig. 4, additional data is reported in Fig. S5–7†). However, in the case of the 0.5%Au–0.5%Pd–0.02%Fe/TiO$_2$ catalyst, no clear signal associated with Fe was measured, which may be attributed to the low metal loading, rather than the inability of the constituent metals to form alloyed structures, which is evidenced by analysis of the 0.5%Au–0.5%Pd–1%Fe/TiO$_2$ catalyst and supported by Mössbauer spectroscopy (Fig. 3 and Table 1). Notably, the immobilised metal nanoparticles were found to exist as random alloys, rather than the core–shell morphologies which have previously been reported for AuPd-based catalysts prepared on oxide supports, *via* similar impregnation methodologies.[33] However, it is important to note that the formation of such core–shell structures typically results from exposure of the catalyst to an oxidative heat treatment, rather than the reductive treatment employed in this study, and the resulting formation of a Pd-oxide outer layer and Au-core.

Time-on-line studies investigating the performance of the key formulations over a reaction time of 180 minutes are reported in Fig. 5 (Fig. S8† compares the activity of the optimal AuPdFe catalyst to alternative trimetallic formulations reported in the literature, under identical reaction conditions, to a reac-

Table 2 Mean particle size, of the as-prepared AuPdFe/TiO$_2$ catalysts, as a function of Fe content

Catalyst	Mean particle size (nm)/(standard deviation)	Productivity/mol$_{H_2O_2}$ kg$_{cat}^{-1}$ h^{-1}
0.5%Au–0.5%Pd/TiO$_2$	4.4 (1.7)	70
0.5%Au–0.5%Pd–0.01%Fe/TiO$_2$	4.6 (2.0)	78
0.5%Au–0.5%Pd–0.02%Fe/TiO$_2$	2.8 (1.1)	122
0.5%Au–0.5%Pd–0.05%Fe/TiO$_2$	4.0 (2.1)	110
0.5%Au–0.5%Pd–0.1%Fe/TiO$_2$	3.8 (2.2)	105
0.5%Au–0.5%Pd–0.5%Fe/TiO$_2$	3.2 (1.3)	94
0.5%Au–0.5%Pd–1.0%Fe/TiO$_2$	3.7 (1.8)	65

H_2O_2 direct synthesis reaction conditions: catalyst (0.01 g), H_2O (2.9 g), MeOH (5.6 g), 5% H_2/CO_2 (420 psi), 25% O_2/CO_2 (160 psi), 0.5 h, 2 °C 1200 rpm. *Note*: catalysts exposed to a reductive heat treatment prior to use (5%H_2/Ar, 400 °C, 4 h, 10 °C min^{-1}).

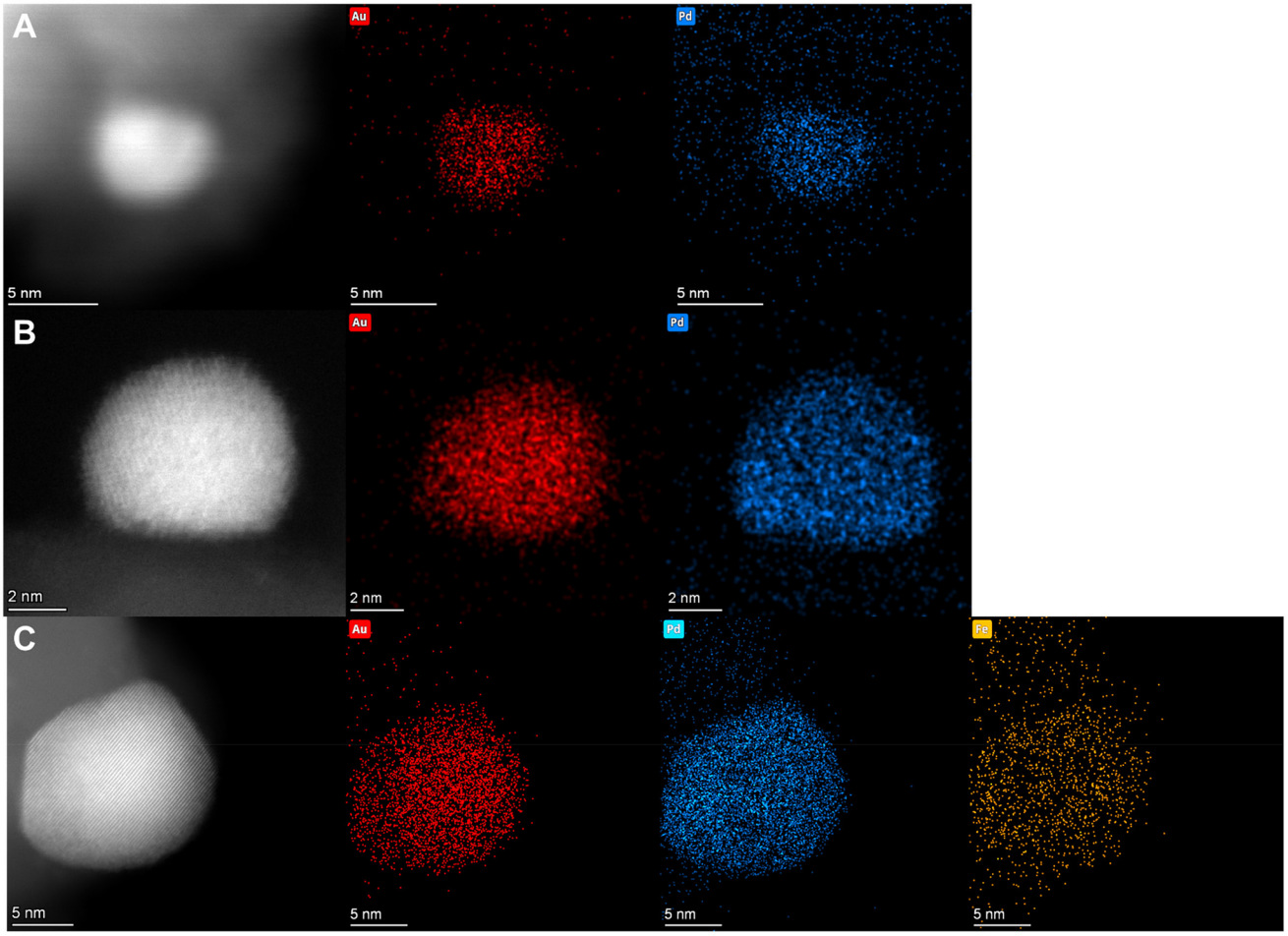

Fig. 4 Representative HAADF-STEM micrographs and complementary EDX analysis of individual alloy nanoparticles in (A) 0.5%Au–0.5%Pd/TiO_2, (B) 0.5%Au–0.5%Pd–0.02%Fe/TiO_2 and (C) 0.5%Au–0.5%Pd–1%Fe/TiO_2. *Note*: catalysts exposed to a reductive heat treatment prior to use (5%H_2/Ar, 400 °C, 4 h, 10 °C min^{-1}).

tion time of 60 min). It should be noted that gaseous reagents were not continuously introduced during these experiments. An analysis of catalyst stability, as evidenced by ICP-MS analysis of post-reaction solutions is reported in Table S5† and indicates the relative stability of these materials. Notably, the inclusion of Fe, particularly at high concentrations, seems to lead to an enhancement in Pd leaching. However, in all cases, the total loss of active species is less than 0.3% of individual metal loadings.

The stark improvement in the reactivity of the 0.5%Au–0.5%Pd–0.02%Fe/TiO_2 catalyst compared to the AuPd or Fe-rich analogues is clear, achieving net concentrations of H_2O_2 between 35 and 45% greater than that offered by alternative formulations, at a reaction time of 60 minutes (Fig. 5A). Notably, at extended reaction times this metric decreases considerably, with the net H_2O_2 concentrations of all three catalysts relatively similar (approx. 0.25 wt%), at a reaction time of 180 minutes. Importantly, the extent of H_2 conversion over the catalytic series (Fig. 5B–D), reveals the near total utilisation of this reagent over the 0.5%Au–0.5%Pd–0.02%Fe/TiO_2 catalyst (>80% H_2 conversion after 180 minutes on-line), compared to that of the alternative formulations (66 and 54% H_2 conversion after 180 minutes for the 0.5%Au–0.5%Pd/TiO_2 and 0.5%Au–0.5%Pd–1%Fe/TiO_2 catalysts, respectively), correlating well with earlier observations that revealed the improved performance of the low Fe-loaded AuPd catalyst are likely attributed to increased activity (*i.e.* a greater extent of H_2 conversion), rather than improved selectivity towards H_2O_2 (Fig. 1 and Tables S2 and S4†).

An evaluation of key catalytic formulations by XPS, over the course of a 180 minute H_2O_2 direct synthesis reaction, is reported in Fig. 6 and indicates that the Pd-speciation present within the as-prepared 0.5%Au–0.5%Pd/TiO_2 and 0.5%Au–0.5%Pd–0.02%Fe/TiO_2 catalysts is maintained to a far greater extent, than over the Fe-rich analogue. Indeed, a total shift towards Pd^0 was detected in the case of the 0.5%Au–0.5%Pd–1.0%Fe/TiO_2 catalyst at a reaction time as short as 5 minutes, revealing the ability of Fe to promote the reduction of Pd. Such observations, when coupled with the known lower selectivity of Pd^0 species, compared to mixed Pd^{2+}–Pd^0 domains, and our

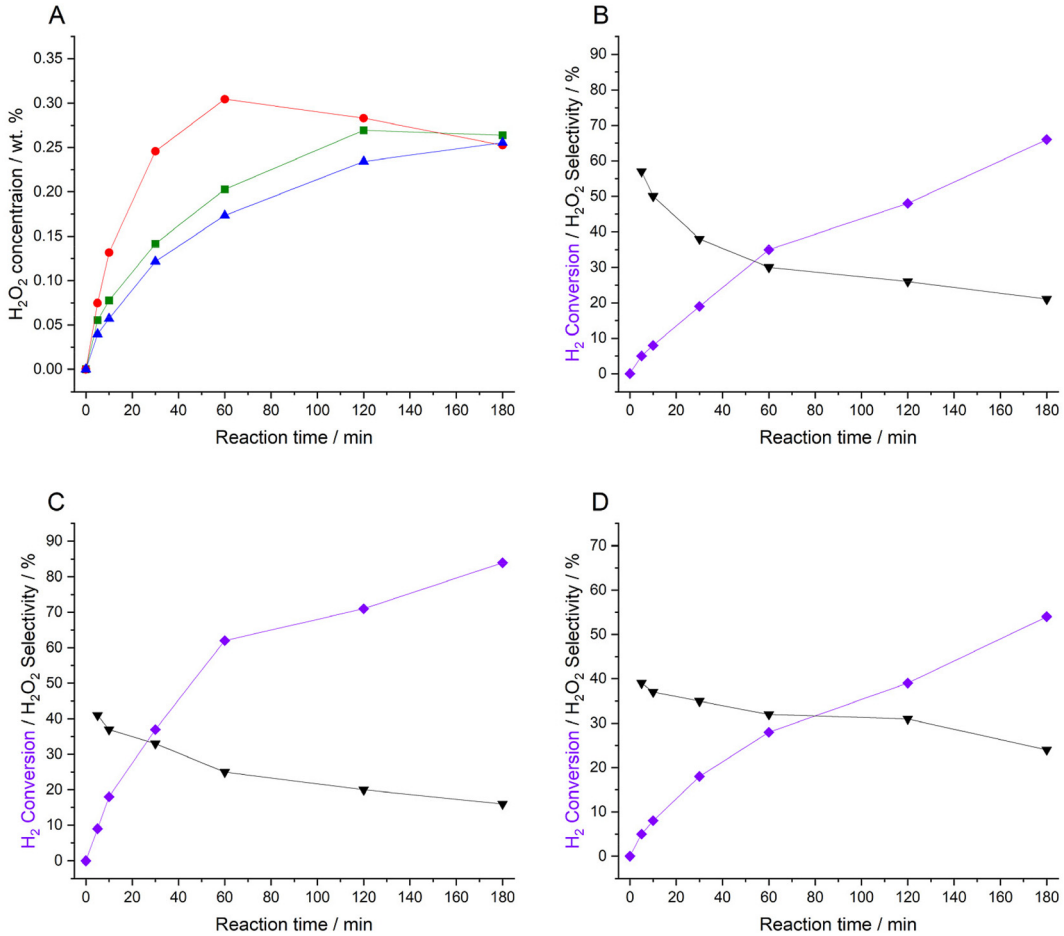

Fig. 5 Comparison of catalytic activity towards the direct synthesis of H_2O_2, as a function of reaction time. (A) Catalytic activity based on net H_2O_2 concentration. Determination of H_2 conversion and H_2O_2 selectivity for the (B) 0.5%Au–0.5%Pd/TiO_2 (C) 0.5%Au–0.5%Pd–0.02%Fe/TiO_2 and (D) 0.5%Au–0.5%Pd–1.0%Fe/TiO_2 catalysts *Key*: 0.5%Au–0.5%Pd/TiO_2 (green squares), 0.5%Au–0.5%Pd–0.02%Fe/TiO_2 (red circles), 0.5%Au–0.5%Pd–1.0%Fe/TiO_2 catalysts (blue triangles) H_2 conversion (purple diamonds), H_2O_2 selectivity (black inverted triangles). H_2O_2 direct synthesis reaction conditions: catalyst (0.01 g), H_2O (2.9 g), MeOH (5.6 g), 5% H_2/CO_2 (420 psi), 25% O_2/CO_2 (160 psi), 2 °C, 1200 rpm.

earlier assessment of H_2 conversion rates and H_2O_2 selectivity may help rationalise the catalytic trends reported in Fig. 1.

With the high rates of H_2 conversion observed over extended reaction times, we subsequently investigated catalytic performance over sequential H_2O_2 synthesis experiments, where gaseous reagents were replaced at intervals of 0.5 h (Fig. 7). The improved performance of the 0.5%Au–0.5%Pd–0.02%Fe/TiO_2 catalyst was again clear, offering a H_2O_2 concentration of 0.76 wt% after five consecutive reactions, approximately 1.8 times greater than that achieved by the bimetallic (0.41 wt%) or Fe-rich (0.44 wt%) analogues. Indeed, the net concentration of H_2O_2 offered by the 0.5%Au–0.5%Pd–0.02% Fe/TiO_2 catalyst is comparable to that achieved by the previously reported and highly active AuPd formulation which has been modified with Pt incorporation,[34] when investigated under identical reaction conditions to those utilised in this work. Indeed, the optimal Fe-containing formulation was found to offer superior activity compared to all of the alternative trimetallic catalysts reported in the literature, when evaluated under identical reaction conditions (Fig. S9†).

With the requirement to re-use a catalyst successfully at the heart of green chemistry, we next evaluated catalytic activity towards H_2O_2 synthesis and H_2O_2 degradation pathways, upon re-use (Table 3). Table S6.† reports metal leaching as determined by ICP-MS analysis of post-direct synthesis reaction solutions. It was found that for all formulations, catalytic activity toward H_2O_2 production decreased upon second use (approx. 32–42% loss of initial activity), with a corresponding loss in H_2 conversion rates. Such deactivation may be attributed to metal leaching, however, our analysis reveals negligible loss of Pd (≤0.12%), and no detectable loss of Au or Fe after 0.5 h of reaction, indicating that alternative factors may contribute to the apparent deactivation of the catalysts upon use in the direct synthesis reaction.

Analysis of key formulations after use in the direct synthesis reaction by TEM is reported in Table 4 (with representative micrographs reported in Fig. S10†), and reveals no considerable change in particle size compared to the as-prepared catalysts (Table 2 and Fig. S3†). Additional evaluation of the spent materials by HAADF-STEM and corresponding EDX analysis

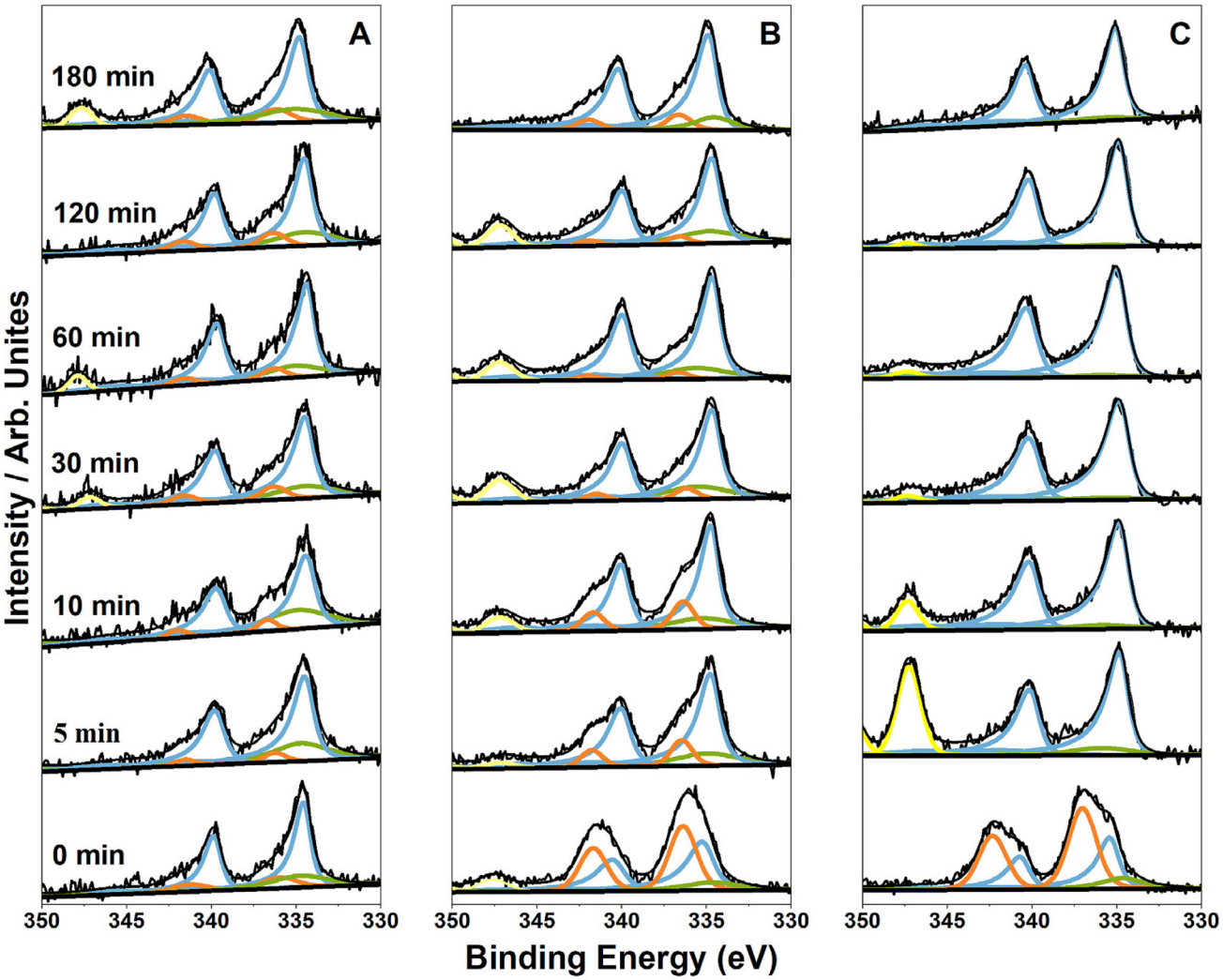

Fig. 6 XPS analysis of the AuPdFe/TiO_2 catalysts, as a function of reaction time. (A) 0.5%Au–0.5%Pd/TiO_2, (B) 0.5%Au–0.5%Pd–0.02%Fe/TiO_2 and (C) 0.5%Au–0.5%Pd–1.0%Fe/TiO_2. *Key*: Au(4d) (green); Pd^0 (blue); Pd^{2+} (orange); Ca^{2+} (yellow). *Note 1*: catalysts exposed to a reductive heat treatment prior to use (5%H_2/Ar, 400 °C, 4 h, 10 °C min^{-1}). Spent catalysts were dried (30 °C, 16 h, under vacuum), prior to XPS analysis. *Note 2*: Ca signal associated with the washing of the spent catalyst with DI water, prior to drying and XPS analysis.

(Fig. S11–13†) corroborates these findings and further indicates that there is no discernible change in nanoparticle composition after use in the direct synthesis reaction (*i.e.* the random alloy nature of the as-prepared materials is retained upon use).

Notably, our previous evaluation of spent catalytic samples by XPS (Fig. 6), revealed the electronic modification of Pd as a result of exposure to H_2O_2 direct synthesis reaction conditions; with a discernible shift in Pd speciation towards Pd^0. Based on this observation alone, and the known lower selectivity, but improved activity of metallic Pd species, one may not have expected the observed decrease in H_2 conversion rates or the lower rates of H_2O_2 degradation observed upon reuse. However, our analysis of spent materials by XPS also reveals a significant loss in chloride content after use in the direct synthesis reaction, (Fig. S14†). Halide ions are well-known promoters for the direct synthesis reaction,[15,35] and their use has typically been shown to result in improved catalytic performance, with this promotive effect often attributed to either the blocking of sites that promote O–O bond scission[36,37] or a reduction in the density of states near the Fermi level, which consequently results in metal surfaces being less reactive for O–O cleavage.[38] More recently, Flaherty and co-workers,[22] proposed that the electronic modification of the solution at the liquid–solid interface induced by the presence of counterions, is largely responsible for the improved activity observed in the presence of Cl^-. Such propositions are indeed compelling. However, regardless of the underlying cause for catalytic promotion in the presence of Cl^-, we can draw a direct correlation between these factors and indeed, such observations are in keeping with earlier studies into AuPd-based catalysts for H_2O_2 synthesis.[15]

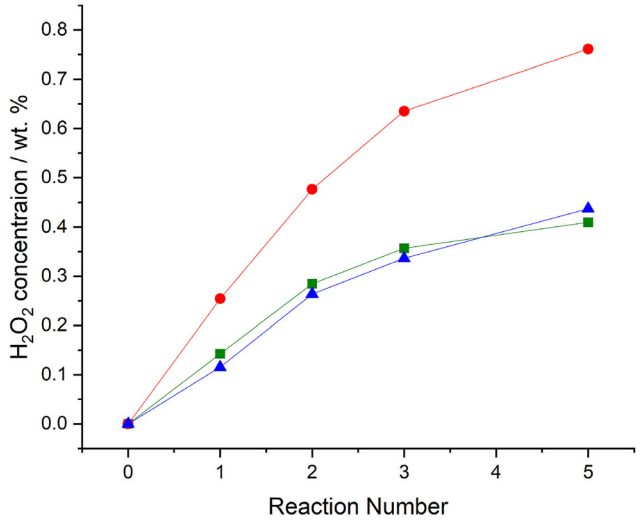

Fig. 7 Comparison of catalytic activity over sequential H_2O_2 synthesis reactions. *Key*: 0.5%Au–0.5%Pd/TiO_2 (green squares), 0.5%Au–0.5%Pd–0.02%Fe/TiO_2 (red circles), and 0.5%Au–0.5%Pd–1.0%Fe/TiO_2 (blue triangles). H_2O_2 direct synthesis reaction conditions: catalyst (0.01 g), H_2O (2.9 g), MeOH (5.6 g), 5% H_2/CO_2 (420 psi), 25% O_2/CO_2 (160 psi), 0.5 h, 2 °C, 1200 rpm.

Based on the presented catalytic data, we subsequently sought to compare the economic potential of the optimal AuPdFe-based catalyst, to other formulations widely studied within the literature, including those based on AuPd and Pd (Fig. 8, with additional data reported in Tables S7A–J†). Notably, such analysis is based on the material cost of key components in the generation of 1 ton of H_2O_2 and does not consider, for example, the additional costs associated with the separation of promoter agents (halides/acids) or the improved reactor lifetime that may result from avoiding their utilisation.[39] Such analysis, perhaps unsurprisingly, indicates that regardless of the catalyst composition a major contributor to cost may be associated with H_2 usage and that based on this, despite the relatively lower cost of the AuPdFe/TiO_2 catalyst ($40.95 per kg), in comparison to a comparable AuPdPt/TiO_2 catalyst ($45.61 per kg), further efforts are required to overcome limitations associated with H_2O_2 selectivity (*i.e* improvements in catalytic activtiy must not lead to a loss in net H_2O_2 production) if the AuPdFe/TiO_2 catalyst is to truly rival alternative formulations.

Table 4 Mean particle size, of key AuPdFe/TiO_2 catalysts, after use in the direct synthesis of H_2O_2

	Mean particle size (nm)/ (standard deviation)	
Catalyst	Fresh	Used
0.5%Au–0.5%Pd/TiO_2	4.4 (1.7)	5.1 (1.9)
0.5%Au–0.5%Pd–0.02%Fe/TiO_2	2.8 (1.1)	5.1 (1.4)
0.5%Au–0.5%Pd–1.0%Fe/TiO_2	3.7 (1.8)	3.6 (1.4)

H_2O_2 direct synthesis reaction conditions: catalyst (0.01 g), H_2O (2.9 g), MeOH (5.6 g), 5% H_2/CO_2 (420 psi), 25% O_2/CO_2 (160 psi), 0.5 h, 2 °C 1200 rpm. *Note*: catalysts exposed to a reductive heat treatment prior to use (5%H_2/Ar, 400 °C, 4 h, 10 °C min^{-1}). Spent samples were dried (30 °C, 16 h, under vacuum).

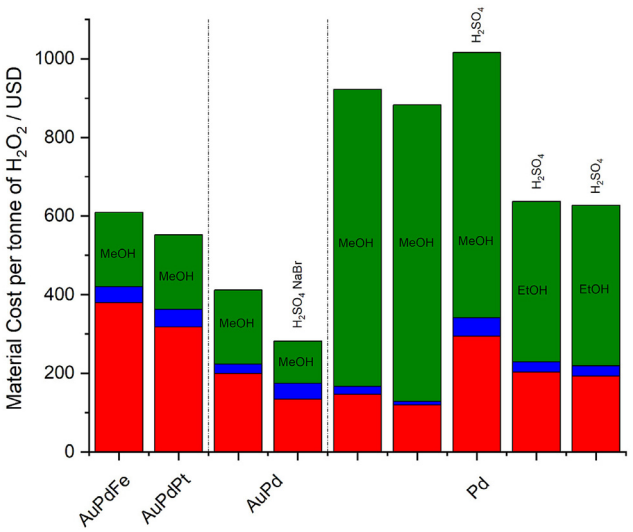

Fig. 8 Techno-economic analysis of the direct synthesis of H_2O_2 over the optimal AuPdFe/TiO_2 catalysts and comparison to alternative formulations. Key: H_2 (red bar), catalyst (blue bar) and organic component of reaction solvent (green bar, ethanol or methanol as indicated), promoters utilised as indicated. Additional data is provided in Tables S7A–J.†

Table 3 Re-usability of AuPdFe/TiO_2 catalysts towards the direct synthesis and subsequent degradation of H_2O_2

	Productivity/ $mol_{H_2O_2}\ kg_{cat}^{-1}\ h^{-1}$		H_2 conv./%		H_2O_2 sel./%		Initial rate of reaction[a]/ $mmol_{H_2O_2}\ mmol_{metal}^{-1}\ min^{-1}$		Degradation/ $mol_{H_2O_2}\ kg_{cat}^{-1}\ h^{-1}$	
Catalyst	Use 1	Use 2	Use 1	Use 2	Use 1	Use 2	Use 1	Use 2	Use 1	Use 2
0.5%Au–0.5%Pd/TiO_2	70	45	19	12	39	37	2.46×10^3	9.71×10^2	208	169
0.5%Au–0.5%Pd–0.02%Fe/TiO_2	122	83	40	22	31	40	3.00×10^3	1.72×10^3	451	431
0.5%Au–0.5%Pd–1.0%Fe/TiO_2	65	38	16	11	42	36	4.65×10^2	1.91×10^2	287	193

H_2O_2 direct synthesis reaction conditions: catalyst (0.01 g), H_2O (2.9 g), MeOH (5.6 g), 5% H_2/CO_2 (420 psi), 25% O_2/CO_2 (160 psi), 0.5 h, 2 °C 1200 rpm. H_2O_2 degradation reaction conditions: catalyst (0.01 g), H_2O_2 (50 wt% 0.69 g) H_2O (2.21 g), MeOH (5.6 g), 5% H_2/CO_2 (420 psi), 0.5 h, 2 °C 1200 rpm. *Note*: [a]reaction rates are calculated based on the as-determined metal content. Spent samples were washed with DI water and dried (30 °C, 16 h, under vacuum), prior to re-use.

Conclusion

The introduction of dopant concentrations of Fe into supported AuPd nanoalloys results in a significant enhancement in catalytic activity towards the direct synthesis of H_2O_2, with the optimal 0.5%Au–0.5%Pd–0.02%Fe/TiO_2 catalyst offering rates of H_2O_2 synthesis greater than that of the parent formulation and competitive with state-of-the-art trimetallic formulations. This improvement is considered to result from the electronic modification of Pd oxidation states upon the addition of Fe, as evidenced by analysis by XPS and CO-DRIFTS. Notably, the enhanced performance of the optimal Fe-containing catalyst can be related to greater H_2 utilisation rather than an inhibition of competitive H_2O_2 degradation pathways, *i.e.* it is increased catalytic reactivity, rather than selectivity, that is responsible for the improvements offered over the parent AuPd bimetallic catalyst. While efforts are still required to overcome concerns around catalytic stability and H_2O_2 selectivity, we consider that these formulations represent a promising basis for further exploration.

Author contributions

R. L., and R. J. L. conducted testing experiments and corresponding data analysis. R. L., D. J. M., T. E. D., D. K. and A. I. D. conducted catalyst characterization and corresponding data processing. R. J. L., A. L., B. R. C. and G. J. H. contributed to the design of the study and provided technical advice and result interpretation. R. J. L. wrote the Manuscript and the ESI,† and all authors commented on and amended both documents. All authors discussed and contributed to the work.

Data availability

All the data is presented in the paper and in the detailed supplementary data.

Conflicts of interest

The authors declare no conflict of interest.

Acknowledgements

The authors wish to thank the Cardiff University electron microscope facility (CCI-EMF), which has been part-funded by the European Regional Development Fund through the Welsh Government and The Wolfson Foundation for the transmission electron microscopy. XPS data collection was performed at the EPSRC National Facility for XPS ('HarwellXPS'), operated by Cardiff University and UCL, under contract No. PR16195. R. L, acknowledges the Chinese Scholarship Council for funding. R. J. L., A. M. and G. J. H. are grateful to The Max Planck Centre for Fundamental Heterogeneous Catalysis (FUNCAT) for financial support.

References

1 R. J. Lewis, K. Ueura, Y. Fukuta, T. E. Davies, D. J. Morgan, C. B. Paris, J. Singleton, J. K. Edwards, S. J. Freakley, Y. Yamamoto and G. J. Hutchings, *Green Chem.*, 2022, **24**, 9496–9507.
2 N. O'Callaghan and J. A. Sullivan, *Appl. Catal., B*, 2014, **146**, 258–266.
3 C. M. Crombie, R. J. Lewis, R. L. Taylor, D. J. Morgan, T. E. Davies, A. Folli, D. M. Murphy, J. K. Edwards, J. Qi, H. Jiang, C. J. Kiely, X. Liu, M. S. Skjøth-Rasmussen and G. J. Hutchings, *ACS Catal.*, 2021, **11**, 2701–2714.
4 A. Santos, R. J. Lewis, D. J. Morgan, T. E. Davies, E. Hampton, P. Gaskin and G. J. Hutchings, *Catal. Sci. Technol.*, 2021, **11**, 7866–7874.
5 S. J. Freakley, Q. He, J. H. Harrhy, L. Lu, D. A. Crole, D. J. Morgan, E. N. Ntainjua, J. K. Edwards, A. F. Carley, A. Y. Borisevich, C. J. Kiely and G. J. Hutchings, *Science*, 2016, **351**, 965.
6 H. Li, Q. Wan, C. Du, J. Zhao, F. Li, Y. Zhang, Y. Zheng, M. Chen, K. H. L. Zhang, J. Huang, G. Fu, S. Lin, X. Huang and H. Xiong, *Nat. Commun.*, 2022, **13**, 6072.
7 J. K. Edwards, B. Solsona, E. N. Ntainjua, A. F. Carley, A. A. Herzing, C. J. Kiely and G. J. Hutchings, *Science*, 2009, **323**, 1037–1041.
8 S. Yu, X. Cheng, Y. Wang, B. Xiao, Y. Xing, J. Ren, Y. Lu, H. Li, C. Zhuang and G. Chen, *Nat. Commun.*, 2022, **13**, 4737.
9 D. Kovačič, R. J. Lewis, C. M. Crombie, D. J. Morgan, T. E. Davies, Á. López-Martín, T. Qin, C. S. Allen, J. K. Edwards, L. Chen, M. S. Skjøth-Rasmussen, X. Liu and G. J. Hutchings, *Green Chem.*, 2023, **25**, 10436–10446.
10 P. Tian, F. Xuan, D. Ding, Y. Sun, X. Xu, W. Li, R. Si, J. Xu and Y. Han, *J. Catal.*, 2020, **385**, 21–29.
11 N. M. Wilson, J. Schröder, P. Priyadarshini, D. T. Bregante, S. Kunz and D. W. Flaherty, *J. Catal.*, 2018, **368**, 261–274.
12 T. Richards, R. J. Lewis, D. J. Morgan and G. J. Hutchings, *Catal. Lett.*, 2022, **153**, 32–40.
13 N. M. Wilson, P. Priyadarshini, S. Kunz and D. W. Flaherty, *J. Catal.*, 2018, **357**, 163.
14 J. Li, T. Ishihara and K. Yoshizawa, *J. Phys. Chem. C*, 2011, **115**, 25359.
15 J. Brehm, R. J. Lewis, D. J. Morgan, T. E. Davies and G. J. Hutchings, *Catal. Lett.*, 2022, **152**, 254–262.
16 R. J. Lewis, K. Ueura, Y. Fukuta, S. J. Freakley, L. Kang, R. Wang, Q. He, J. K. Edwards, D. J. Morgan, Y. Yamamoto and G. J. Hutchings, *ChemCatChem*, 2019, **11**, 1673.
17 J. K. Edwards, J. Pritchard, L. Lu, M. Piccinini, G. Shaw, A. F. Carley, D. J. Morgan, C. J. Kiely and G. J. Hutchings, *Angew. Chem., Int. Ed.*, 2014, **53**, 2381.
18 A. Barnes, R. J. Lewis, D. J. Morgan, T. E. Davies and G. J. Hutchings, *Catal. Sci. Technol.*, 2022, **12**, 1986–1995.

19 A. Barnes, R. J. Lewis, D. J. Morgan, T. E. Davies and G. J. Hutchings, *Catalysts*, 2022, **12**, 1396.
20 A. Santos, R. J. Lewis, G. Malta, A. G. R. Howe, D. J. Morgan, E. Hampton, P. Gaskin and G. J. Hutchings, *Ind. Eng. Chem. Res.*, 2019, **58**, 12623–12631.
21 J. K. Edwards, A. Thomas, A. F. Carley, A. A. Herzing, C. J. Kiely and G. J. Hutchings, *Green Chem.*, 2008, **10**(4), 388.
22 N. M. Wilson and D. W. Flaherty, *J. Am. Chem. Soc.*, 2016, **138**, 574.
23 Z. Klencsár, *Nucl. Instrum. Methods Phys. Res., Sect. B*, 1997, **129**, 527–533.
24 L. Ouyang, P. Tian, G. Da, X. Xu, C. Ao, T. Chen, R. Si, J. Xu and Y. Han, *J. Catal.*, 2015, **321**, 70–80.
25 R. Vanleerberghe, E. de Grave, R. E. Vandenberghe and G. G. Robbrecht, *J. Phys. Colloques*, 1980, **41**, 179–180.
26 S. Cho, S. M. Kauzlarich, J. Olamit, K. Liu, F. Grandjean, L. Rebbouh and G. J. Long, *J. Appl. Phys.*, 2004, **95**, 6804–6806.
27 J. Brehm, R. J. Lewis, T. Richards, T. Qin, D. J. Morgan, T. E. Davies, L. Chen, X. Liu and G. J. Hutchings, *ACS Catal.*, 2022, **19**, 11776–11789.
28 J. H. Carter, S. Althahban, E. Nowicka, S. J. Freakley, D. J. Morgan, P. M. Shah, S. Golunski, C. J. Kiely and G. J. Hutchings, *ACS Catal.*, 2016, **6**, 6623–6633.
29 G. Cerrato, L. Marchese and C. Morterra, *Appl. Surf. Sci.*, 1993, **70–71**, 200–205.
30 I. X. Green, W. Tang, M. Neurock and J. T. Yates, *Science*, 2011, **333**, 736–739.
31 M. A. P. Dekkers, M. J. Lippits and B. E. Nieuwenhuys, *Catal. Lett.*, 1998, **56**, 195–197.
32 B. Zheng, G. Liu, L. Geng, J. Cui, S. Wu, P. Wu, M. Jia, W. Yan and W. Zhang, *Catal. Sci. Technol.*, 2016, **6**, 1546–1554.
33 J. K. Edwards, A. F. Carley, A. A. Herzing, C. J. Kiely and G. J. Hutchings, *Faraday Discuss.*, 2008, **138**, 225.
34 X. Gong, R. J. Lewis, S. Zhou, D. J. Morgan, T. E. Davies, X. Liu, C. J. Kiely, B. Zong and G. J. Hutchings, *Catal. Sci. Technol.*, 2020, **10**, 4635.
35 E. N. Ntainjua, M. Piccinini, J. C. Pritchard, Q. He, J. K. Edwards, A. F. Carley, J. A. Moulijn, C. J. Kiely and G. J. Hutchings, *ChemCatChem*, 2009, **1**, 479.
36 J. H. Lunsford, *J. Catal.*, 2003, **216**, 455.
37 V. R. Choudhary and C. J. Samanta, *J. Catal.*, 2006, **238**, 28.
38 M. Hohenegger, E. Bechtold and R. Schennach, *Surf. Sci.*, 1998, **412–413**, 184–191.
39 G. Gao, Y. Tian, X. Gong, Z. Pan, K. Yang and B. Zong, *Chin. J. Catal.*, 2020, **41**(7), 1039–1047.